

Biological glass fibers: Correlation between optical and structural properties

Joanna Aizenberg*,†, Vikram C. Sundar*, Andrew D. Yablon†, James C. Weaver§, and Gang Chen*

*Bell Laboratories/Lucent Technologies, Murray Hill, NJ 07974; †OFS Laboratories, Murray Hill, NJ 07974; and §Institute for Collaborative Biotechnologies and Materials Research Laboratory, University of California, Santa Barbara, CA 93106

Communicated by J. Anthony Tyson, Bell Laboratories/Lucent Technologies, Murray Hill, NJ, January 16, 2004 (received for review November 24, 2003)

Biological systems have, through the course of time, evolved unique solutions for complex optical problems. These solutions are often achieved through a sophisticated control of fine structural features. Here we present a detailed study of the optical properties of basalia spicules from the glass sponge *Euplectella aspergillum* and reconcile them with structural characteristics. We show these biosilica fibers to have a distinctive layered design with specific compositional variations in the glass/organic composite and a corresponding nonuniform refractive index profile with a high-index core and a low-index cladding. The spicules can function as single-mode, few-mode, or multimode fibers, with spines serving as illumination points along the spicule shaft. The presence of a lens-like structure at the end of the fiber increases its light-collecting efficiency. Although free-space coupling experiments emphasize the similarity of these spicules to commercial optical fibers, the absence of any birefringence, the presence of technologically inaccessible dopants in the fibers, and their improved mechanical properties highlight the advantages of the low-temperature synthesis used by biology to construct these remarkable structures.

The class Hexactinellida, of the phylum Porifera, the so-called glass sponges of the deep sea, consists of >500 extant species as well as a considerable number of extinct members extending from the early Cambrian period to the present (1). Their mineralized skeletons have been shown to be composed of spicules of amorphous hydrated silica deposited around a proteinaceous axial filament. Depending on the particular species, spicule morphology, and location within the sponge, the function of these spicules varies from a predation deterrent to providing the bulk of the sponge's mechanical rigidity (2, 3). In other instances, the spicules are modified into elaborate fibrous anchoring structures that permit the successful colonization on soft sediments (2, 3). More recent work has investigated potential optical roles for these fibers (4–7). The presence of apex type structures on the top of spicules from the hexactinellid sponge *Rosella racovitzae*, for example, was shown to enhance the light acceptance angles into these large fibers, thus considerably improving their ability to effectively channel ambient light (4).

Recently, we suggested that spicules from another hexactinellid sponge, *Euplectella aspergillum* (Venus' flower basket), have fiber-optical characteristics similar to those of commercial telecommunications fibers (6). The *Euplectella* species live at depths ranging from 35 to 5,000 m in a cold environment, frequently with no ambient sunlight (8–10). The mineralized skeleton of *E. aspergillum* consists of an intricate cylindrical cage-like construction composed of a lattice of spicules imbedded in a secondarily deposited silica matrix that provides extended structural rigidity (Fig. 1a). The cage is typically inhabited by a pair of symbiotic shrimps. At the base of the sponge are the basalia, a network of anchorage spicules with recurved barbs (Fig. 1b) that secure the sponge in soft sediments (11), the typical habitat for this species. It is these spicules that form the focus of the current study. The basalia (anchorage) spicules are generally 5–15 cm in length and between 40 and 70 μ m in diameter. The smooth distal portion of each spicule (Fig. 1c) either radiates away from this basal

holdfast apparatus in a crown-like fashion or is incorporated into the longitudinal (vertical) spicular struts of the skeletal framework.

In this work, we provide a detailed study of the optical properties of these biosilica fibers and correlate them to structural and compositional features. Structural and chemical-etch analyses indicate compositional complexity, with specific variations in dopant content, organic composition, and degree of silica condensation within the distinct domains of the spicule. Free space coupling of laser light as well as white light is used to study the waveguiding properties of the spicules. We demonstrate that they are remarkably similar to commercial silica optical fibers and are capable of forming an effective fiber-optical network. Advantages of the low-temperature synthesis of these optical fibers at biological conditions are shown to include increased fracture toughness, the absence of residual stress, and the use of refractive index-raising dopants that are inaccessible in current technology.

Materials and Methods

Structural and Elemental Analysis. Basalia spicules were carefully removed from specimens of *E. aspergillum*. The fibers were first frozen in liquid nitrogen and then fractured. Thereafter, the spicules were treated with 5% hydrogen fluoride solution or 5% sodium hypochlorite solution for 10 min, rinsed extensively in water and ethanol, and blow-dried. Both of these techniques (HF and NaOCl etching) have, with slight modifications, previously proved useful in the elucidation of siliceous spicule substructure (12, 13). The fibers were then mounted onto scanning electron microscope (SEM) aluminum stubs by using conductive carbon tape, sputter-coated with \sim 10–20 nm of gold (Au), and imaged in a JEOL JSM 5600LV SEM (operating voltage 15 keV, working distance 12 mm). Alternatively, multiple spicules were placed within an epoxide monomer (Epoxy hardener, Electron Microscopy Products, refractive index 1.571), which was then thermally cured. The resulting solid cylindrical block was sectioned into 5- to 8-mm-thick pieces, each of which had multiple embedded spicules. Elemental composition was then obtained by using an energy-dispersive x-ray (EDX) module attached to the SEM. Gold-coated specimens were analyzed for the presence of carbon, and carbon-coated specimens were analyzed for the presence of Na, K, Mg, Ca, Hg, and Sr.

Interferometric Analysis of Biological Fibers. A Mach-Zehnder interferometer incorporated within a transmitted light microscope enabled measurement of the fiber's refractive index relative to matching oil with a 1- μ m spatial resolution. Inside the microscope, a beam splitter divided the output of a 546-nm mercury arc lamp source into a sample beam and a reference beam. The sample beam was sent transversely through a whole fiber immersed in a refractive index-matching oil (Cargille series

Abbreviations: SEM, scanning electron microscope; EDX, energy-dispersive x-ray; OF, organic filament; CC, central cylinder; SS, striated shell.

*To whom correspondence should be addressed. E-mail: jaizenberg@lucent.com.

© 2004 by The National Academy of Sciences of the USA



Fig. 1. (a) Photograph of a typical specimen of *E. aspergillum*, showing the lattice-like skeleton of fused siliceous spicules and a crown-like organization of basalia at the base. (b–d) SEM micrographs of the spined proximal region (b) and the smooth distal region of a basalia spicule (c) and its apical process (d). The SEM micrographs are related to a schematic representation of an individual spicule from the anchoring region (Center).

AA, index of 1.43 at 589 nm) and imaged with a $\times 100$ objective. The reference beam was sent through an identical index-matching oil and imaged with a similar objective. Subsequent combining of the two beams resulted in an interferogram from which the refractive index profile was extracted by using an algorithm from Marcuse developed for axisymmetric fibers (14). To measure the optical anisotropy of the fibers, we varied the polarization of the light and compared the refractive index of the fiber along the transverse and axial directions (15).

Transmission Optical Characterization of Fibers. A single freeze-fractured fiber section (5–8 cm in length) was mounted on standard optical fiber mounts. Light was free-space coupled into one end of the fiber section with a multimode fiber coupled to an Ando AQ-4303 white light source or a red laser diode on the other end. Uncoupled light was rejected through the use of an opaque fixative, and the highly divergent output from the spicule was collected through an objective and focused onto a screen. The intensity of the observed spot was very sensitive to the exact position as well as the relative angle between the input fiber and the spicule's input end. The output on a screen was optimized by using the red laser light, and the same configuration was then used for the white light. These fibers were imaged either end-on by using a charge-coupled device (CCD) camera with an objective ($\times 20$ magnification), or along the length of the fiber by using a CCD camera attached to a stereoscope ($\times 2$ magnification). Light coupled out of the ends of the fiber was imaged and dispersed onto a spectrometer.

Results

The microscopy study of the spicule structure showed that most of their distal surface is smooth and featureless (Fig. 1c), with

numerous barb-like spines located proximally (Fig. 1b). At the end of the barbed portion of each spicule is a terminal spinous process (Fig. 1d). The “stress-free” native cross sections of the basalia spicules are relatively smooth and, remarkably, show no indication of structural boundaries (Fig. 2a Inset). Under stress (e.g., being mechanically cleaved), however, the spicules reveal a characteristic layered architecture (12) with three distinct regions: an $\sim 0.5\text{-}\mu\text{m}$ -wide organic axial filament (OF) running through a solid, smooth, 15- to $25\text{-}\mu\text{m}$ -wide central cylinder (CC), which is embedded in a striated shell (SS) composed of a series of equally spaced, 0.8- to $1.0\text{-}\mu\text{m}$ -wide layers (Fig. 2a).

To gain additional insight into the structure and composition of these spicules, we performed a series of etching experiments (16) with either HF (12) or NaOCl (13). HF treatment produced spicules with a characteristic, hollow, conical morphology (Fig. 2b). The core of the central cylinder corroded first, revealing an $\approx 2\text{-}\mu\text{m}$ hole with an OF at its center (Fig. 2b Inset). Progressive outward etching of the laminated outer portion occurred next, producing gradually receding layers that surrounded the protruding CC. Because the etching rate in HF varies considerably as a function of the degree of silica condensation, dopant content, and surface area available for chemical attack (17), such differential etching experiments hinted at variations in the composition of the spicules. Our results suggested that the spicules consist of a hydrated and/or heavily doped silica core with an enclosed OF, and silica layers with progressively decreasing organic content and/or hydration, as one travels from the CC to the spicule periphery.

Variations in the fine structure across the spicule were further investigated by treatment with NaOCl (13, 16). After exposure to this alkaline etchant, selective removal of the OF was observed and the smooth surfaces of the spicules became considerably coarsened. These surfaces appeared to be composed of silica spheres that gradually increased in size from <50 nm in the CC region to ≈ 200 nm in the outermost layers of the SS (Fig. 2c). Preferential etching at the interfaces between the shell layers (see arrows in Fig. 2c) was indicative of the presence of organic “glue” holding the shells together. Vestiges of these organic films are seen in Inset to Fig. 2c.

EDX elemental mapping of the spicule's sections showed a clear carbon signal in the center of the fiber, most likely arising from the OF (Fig. 2d Left). A higher concentration of carbon was seen in the CC region than in the SS region. An enhanced presence of Hg and Na was detected throughout the spicule and, in particular, in the core region (Fig. 2d Right). While small quantities of carbon (most likely, in the form of intrasilica organic molecules) were detected in the CC region, it seems unlikely that its presence alone could be responsible for the observed differences in etchant reactivity for the distinct spicule regions. The inclusion of inorganic dopants and variability in the degree of silica condensation are probably also contributing factors (12, 13, 17).

The observed correlation between the variations in the chemical composition of the spicules and their nonuniform refractive index profile prompted a more detailed analysis of the optical properties of these fibers through the use of interferometry (14). Because this technique is nondestructive and provides radial as well as axial resolution of a spicule's refractive index, it is ideally suited for extracting structure–function correlations in these spicules. The measurements were performed at different locations along the spicule's length. An example of a typical interferogram obtained is provided in Fig. 3a (6). The variations in refractive index manifest themselves as variations in the vertical position of the interferometric fringes (dark horizontal bands) in Fig. 3a. The quantitative refractive index values derived from the interferograms and plotted as a function of the position in the fiber's cross section are shown in Fig. 3b.

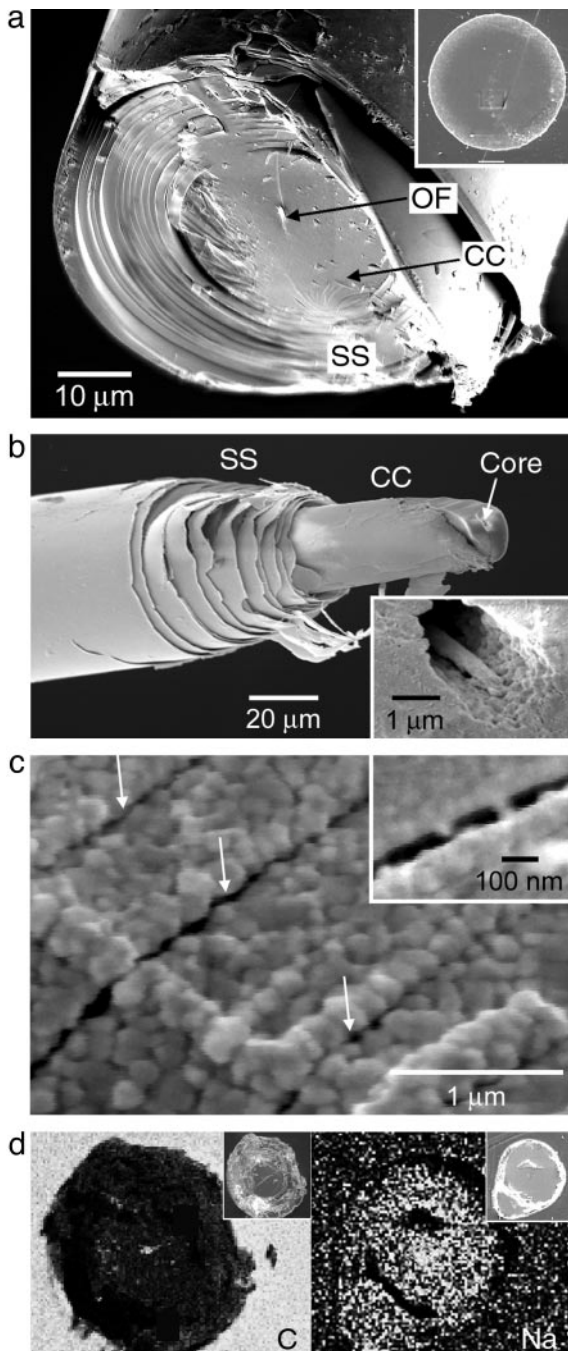


Fig. 2. Structural and compositional characterization of the basalia spicules. (a) SEM image of a mechanically cleaved freestanding spicule, revealing an axial organic filament (OF), a smooth central cylinder (CC), and a striated shell region (SS). (Inset) SEM image of a similar spicule that was gently polished after embedding in an epoxide. A smooth homogeneous cross section is seen. (b) Etch figures produced after HF treatment. The exposed CC region with the hollow core (indicated by an arrow) and surrounded by a receding series of SS layers is seen. (Inset) High-magnification scanning electron micrograph of the etched core region ($\approx 2 \mu\text{m}$ in diameter), exposing the OF. (c) Etch figures produced after bleach (NaOCl) treatment reveal that the spicule's building blocks are silica spheres. Arrows indicate the interfaces between the shell layers, from which organic material is selectively removed. (Inset) Magnified view of the interface, revealing remnants of the organic bridges. (d) Left) EDX carbon map of Micrотome-cut spicule cross section highlights the presence of an OF. Note that the carbon content in the CC region is higher than that in the SS region. (Right) EDX sodium map indicates an enhanced concentration of sodium ions within the spicule cross section, with the highest density of Na occurring in the $2\text{-}\mu\text{m}$ core. (Insets) SEM images of the corresponding spicules.

Although the absolute values of the refractive index vary along the length of the fiber, the same pattern is evident in all regions. First, there is a high refractive index core ($1\text{--}2 \mu\text{m}$ in diameter) that corresponds to the Na-doped region in EDX, in which the spicule's refractive index (1.45–1.48) is very close to (or higher! than) that of vitreous silica of 1.458 (Fig. 3b). Second, surrounding this core is a larger cylindrical tube ($15\text{--}25 \mu\text{m}$ in diameter), which has a lower refractive index (as low as 1.425) than the Na-doped core. This cylinder corresponds well to the CC region detected in the structural studies, and its reduced refractive index could be explained by its high organic content and/or low degree of silica condensation. Last, the outer portion of the spicule shows a progressively increasing refractive index (from 1.433 to 1.438), in agreement with the observed gradual composition variation (Fig. 2b) and the increasing diameter of the silica spheres in the SS layers. An oscillatory pattern of the refractive index in this region is consistent with the presence of well defined bands of organic molecules, seen as bridging ligands at the interfaces between the layers (see Fig. 2c). The finite optical resolution of the refractive index measurement (on the order of $1 \mu\text{m}$) limits the accurate spatial resolution of the oscillatory pattern.

Varnham *et al.* (15) showed how the difference between refractive index measurements acquired with axial and transverse polarizations (i.e., the birefringence) could be used to measure residual thermal stresses in commercial optical fiber preforms or fibers. Polarization-specific refractive index measurements of the spicules are summarized in Fig. 3c. Although the absolute refractive index in the core region for either polarization was substantially higher than that of vitreous silica (as high as 1.48), along the cross section of the spicule the refractive index profiles for the different polarizations of light were largely identical. Even in the core, the observed difference in refractive index of 0.002 was at the detection threshold of the interferometric index profiler.

The revealed characteristic “core-cladding” structure of the spicules raised the interesting possibility that these biologically formed fibers may possess waveguiding properties, and their core could carry a single-mode optical signal (6). Various light-coupling experiments were performed to address this question (Fig. 4). Indeed, experiments with spicule sections embedded in epoxide and coupled to white light indicate that light is transported predominantly through the core of the spicule and a narrow region surrounding the core and that not much light is transported through the cladding layer (i.e., either the striated shell region or the central cylinder) (Fig. 4b), as would be expected in a single/few-mode optical fiber. Such waveguiding characteristics of these spicules result from the raised refractive index of the epoxide (≈ 1.57) relative to that of the cladding.

In natural environments, however, the spicules are surrounded by seawater. The refractive index difference (Δn_m) between the spicule's biosilica (≈ 1.43) and the surroundings (≈ 1.33) is, therefore, much larger than the refractive index difference (Δn_s) between the core and the cladding (Fig. 3d). Moreover, the cladding diameter is much larger than the core diameter. These facts suggest that in natural environments, it is far more likely that the light would be strongly confined within the entire spicule, which should then function as a multimode fiber. To better approximate biological conditions, red laser light was free-space coupled from an optical fiber into the spicule in air (Fig. 4a). Light guided through the spicule was clearly visible and imaged onto a screen through an objective (Fig. 4a Inset). When white light was coupled into the spicule through this optimized setup, the spicule behaved as a highly multimode light guide; that is, most of the light traveling inside the fiber filled the entire cladding and was confined by the outer surface of the fiber (Fig. 4c), because of the enhanced refractive index contrast between the spicule and the surroundings (air).

The light-coupling experiments with the spined sections of the spicules showed that the light is out-coupled at the spined positions along the spicule shaft (Fig. 4*d*). Our interferometric analysis (Fig. 4*d Inset*) indicated that the striations and cladding refractive index seen in the shell layer extend into the spined region as well. Light confined to the cladding of the spicule by total internal reflection diffuses out at the location of the spines. At the tips of these spines, the local angle of the interface is nearly perpendicular to the transported light wave and allows for the escape of light into the surrounding seawater. Thus, light that is being transported in the cladding could be efficiently coupled into the spines and these spines could serve as tiny “points of illumination” along the spicule shaft.

The waveguiding efficiency generally increased when the light was coupled through the spicule’s end bearing the terminal head structure (Fig. 1*d*). The frequent shearing of the anchor spicules from the basal portion of the skeleton and the frequent lack of the intact recurved spicule termini may help explain why some spicules exhibit better optical conductance properties than others, and thus raise intriguing questions for the role of the terminal head as a potential light-collecting, lens-like structure (4, 18).

Discussion

To the best of our knowledge, this work is the first detailed optical study that explicitly analyzes the refractive index profile within biologically formed silica fibers and relates the optical properties to the spicule’s unique structural and compositional features. We show the spicules to have a characteristic design that encompasses a high-index core composed of Na-doped silica, with the refractive index higher than that of vitreous silica, and a low-index cladding composed of an organic-material-containing, hydrated silica cylinder wrapped in organically glued multiple silica layers, conceivably with an increasing degree of condensation. We highlight the remarkable similarities between these spicules and commercial optical fibers used for telecommunications (19); that is, they are formed from the same material, have similar dimensions and a nonuniform refractive index profile with a high-index core and a low-index cladding, and therefore can function both as a single-mode fiber or a multimode fiber, depending on the refractive index of the surroundings.

These spicules, however, offer a number of advantages over the typical telecommunication fibers. First are their original structural features and the associated enhanced fracture toughness. The main failure mode of commercial silica fibers is fracture resulting from crack growth. When bent or twisted, the fibers experience extreme mechanical stresses at large radial positions. The presence of the characteristic lamellar layers in the exterior regions of these spicules connected by bridging organic ligands provides an effective crack-arresting mechanism. Such a general structural motif is highly beneficial in increasing the strength of composite materials (20) and has been studied extensively in other biological systems (21–23). While previous papers on siliceous sponge spicules reported a layered morphology, it was suggested to arise from mechanical stress, and a constant chemical composition across the spicule was concluded (5, 21). Our work unequivocally demonstrates that the characteristic layered morphology of these spicules is not just the result of mechanical cleaving, but is also intimately tied to their nonuniform chemical composition, which is, in turn, manifested in distinctive optical properties.

Other interesting design elements include terminal lens-like extensions located proximally and barb-like spines located along the spicule shaft. The presence of these lens structures at the end of the biofibers improves the light-collecting efficiency (4). The demonstrated out-coupling of thus-enhanced light through the spicule tips and the spined regions offers an effective fiber-

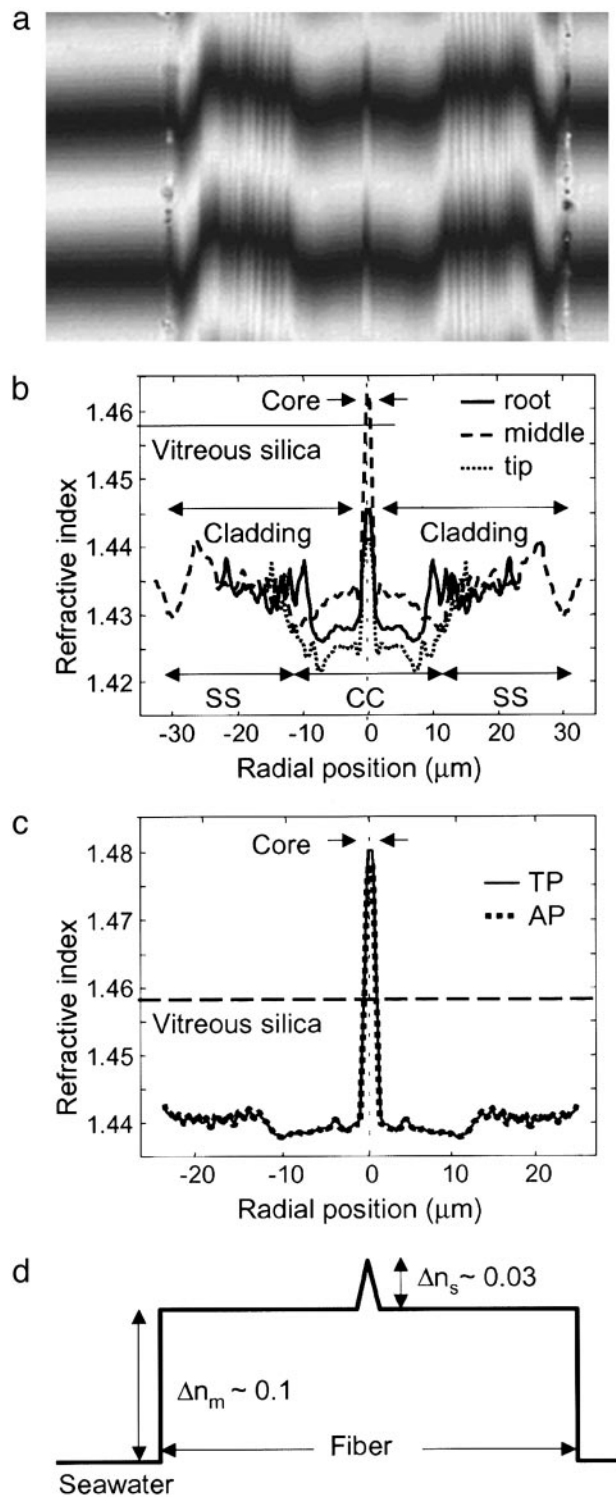


Fig. 3. Interferometric refractive index analysis of spicules. (a) Typical interferogram of an individual spicule. (b) Quantitative refractive index values extracted from interferograms of spicules similar to those in *a*. (c) Polarization-specific refractive index measurements reveal negligible differences in the refractive index of fiber for either transversely or axially polarized light. (d) Schematic refractive index profile of the spicule in seawater. The structure can be considered as a single-mode fiber with a low refractive index cladding, which comprises both the CC and the SS regions, and a high refractive index core. Alternatively, because of the large refractive index difference between silica and seawater, the entire spicule can be considered as a high refractive index core region surrounded by a lower refractive index seawater cladding, thus forming a multimode waveguide.

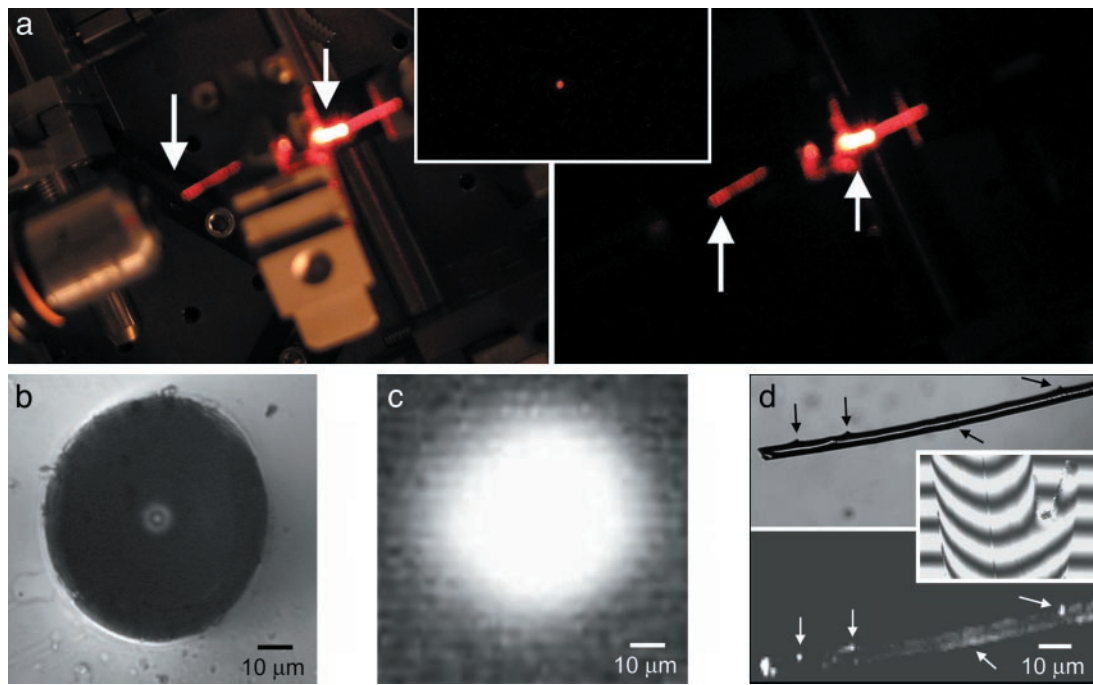


Fig. 4. Light-coupling experiments. (a) Free-space coupling of light to a free fractured spicule results in the entire fiber being illuminated. Right and Left are images of the experimental setup in the presence and absence of room light. Referenced with arrows (a and b) are the input and output ends of the spicule. (Inset) Output of the spicule imaged on a screen. (b) Transmission optical image of a spicule embedded in epoxide. The 2- μm core region is brighter than the cladding, showing that the fiber acts as a single-mode (few-mode) waveguide. (c) Transmission image of a freestanding spicule. Entire fiber is lit up, showing that the fiber acts as a highly multimode waveguide. (d) Light coupling into the spined regions of the fiber. (Upper) Optical micrograph of the original fiber with the spine positions labeled with arrows. (Lower) Optical image of the same fiber upon free-space coupling of white light into the fiber. Although the bulk of the fiber is substantially dark, select illumination points corresponding to the spine positions are observed. (Inset) Interferometric image showing the extension of the striated shell into the spined region of the spicule.

optical network with selected illumination points along the length of the crown-like fibrous network surrounding the cylindrical skeletal lattice.

Second, the formation of the biosilica fibers occurs at ambient temperatures and pressures. Their complex structure and composition are encoded in the organism and are controlled by specialized organic molecules and cells. The low-temperature formation of silica in organisms, as an alternative to the high-temperature technological process (24), is a subject of extensive studies (25–32). It has been shown that proteinaceous axial filaments isolated from the Eastern Pacific demosponge *Tethya aurantia* and their constituent proteins, silicateins (extracted from the filaments or produced from recombinant DNA templates) were effective in the *in vitro* induction of hydrolysis and polycondensation of silicon alkoxides to yield silica at ambient temperature and pressure and neutral pH (25, 26, 30–32). Previous work investigating the mechanisms of silification in diatoms suggested that the formation of silica nanoparticles is directed by specific polycationic peptides, silaffins (27–29).

The low-temperature synthesis brings about an extremely important feature: the ability to effectively dope the structure with impurities that increase the refractive index of silica. Our elemental analysis showed, for example, the presence of sodium ions in the entire fiber, particularly in the core. Sodium ions (and many other additives) are not commercially viable optical fiber dopants because of manufacturing challenges, including devitrification at high processing temperatures. In the case of these spicules, however, the presence of sodium ions results in the increase of the refractive index to values approaching and even exceeding that of vitreous silica.

The transmission loss of commercial fibers is primarily limited by Rayleigh scattering due to small density fluctuations inevi-

tably distributed in the vitreous silica, therefore a fiber composed of a collection of vitreous silica nanospheres would likely exhibit much higher amounts of Rayleigh scattering and be impractical for long-distance low-loss signal transmission applications. However, other specialty commercial fibers, such as rare-earth-doped fibers, are used to amplify optical signals over short lengths of fiber (<10 m), so nanospheres might not be a significant disadvantage and room temperature fabrication might permit the inclusion of novel useful dopant species.

Another advantage of the low-temperature synthesis is evidenced in the lack of the polarization dependence on the refractive index. Birefringence in commercially prepared fibers often occurs as a result of the residual thermal stresses in the fibers upon their cooling (15). Ambient condition formation of the spicules in biological environments prevents the development of any residual thermal stress.

We wonder whether the observed remarkable fiber-optical capabilities of these spicules are actually used by this species in the wild or are accidental, a fascinating question worthy of further investigation. We can only speculate at this moment that these silica spicules, beyond structural anchorage support, *may* also provide an intricate network of naturally formed optical fibers. While fibrous spicules in the shallower-dwelling *Rosella racovitzae* have been postulated to act as an effective light-collecting system, delivering sunlight to the sponge's presumably endosymbiotic algae (4, 5, 7), we do not yet know whether a similar relationship might exist in *Euplectella*. Indeed, in the presence of sufficient light, a variety of optical elements, ranging from iridescent gratings to efficient microlens arrays, have been developed by nature (18, 33, 34). The hexactenellid sponge *E. aspergillum*, however, typically occurs at depths at which the paucity of ambient sunlight, high pressure, and hydrothermal

vents lead to bio- or chemiluminescence being the only feasible sources of illumination (35–37).

Our results suggest that if such sources exist within or in close association to the basalia of *E. aspergillum*, their light might be efficiently used and distributed by the sponge. Such a fiber-optical lamp might potentially act as an attractant for larval or juvenile stages of these organisms and symbiotic shrimp to the host sponge. Whether and how the latter are adapted for photoreception presents another unexplored question (18, 36). Further analysis might also examine the possible presence of bioluminescent microorganisms (35–37) that live symbiotically at depths typically inhabited by this organism and explore the potentially mutualistic benefits for both species involved in these apparent symbioses.

We can also, at this point, not rule out the possibility that the observed fiber-optic properties of these spicules may in fact not be biologically relevant and may merely be a secondary consequence of the evolution of a flexible fracture-resistant skeletal system successful for the colonization on soft substrates (11).

1. Reiswig, H. M. & Mackie, G. O. (1983) *Philos. Trans. R. Soc. London B* **301**, 419–428.
2. Koehl, M. A. R. (1982) *J. Exp. Biol.* **98**, 239–244.
3. Simpson, T. L. (1984) *The Cell Biology of Sponges* (Springer, New York).
4. Cattaneo-Vietti, R., Bavestrello, G., Cerrano, C., Sara, M., Benatti, U., Giovine, M. & Gaino, E. (1996) *Nature* **383**, 397–398.
5. Sarikaya, M., Fong, H., Sunderland, N., Flinn, B. D., Mayer, G., Mescher, A. & Gaino, E. (2001) *J. Mater. Res.* **16**, 1420–1428.
6. Sundar, V. C., Yablon, A. D., Grazul, J. L., Ilan, M. & Aizenberg, J. (2003) *Nature* **424**, 899–900.
7. Gaino, G. & Sarà, M. (1994) *Marine Ecol. Prog. Ser.* **108**, 147–151.
8. Perry, C. C. & Keeling-Tucker, T. (2000) *J. Biol. Inorg. Chem.* **5**, 537–550.
9. Beaulieu, S. E. (2001) *Marine Biol.* **138**, 803–817.
10. Saito, T. & Takeda, M. (2003) *J. Marine Biol. Assoc. U.K.* **83**, 119–131.
11. Lévi, C., Barton, J. L., Guillemet, C., Le Bras, E. & Lehude, P. (1989) *J. Mater. Sci. Lett.* **8**, 337–339.
12. Schwab, D. W. & Shore, R. E. (1971) *Nature* **232**, 501–504.
13. Weaver, J. C., Pietrasanta, L. I., Hedin, N., Chmelka, B., Hansma, P. K. & Morse, D. E. (2003) *J. Struct. Biol.* **144**, 271–281.
14. Marcuse D. (1981) *Principles of Optical Fiber Measurements* (Academic, New York).
15. Varnham, M. P., Poole, S. B. & Payne, D. N. (1984) *Electron. Lett.* **20**, 1034–1035.
16. Aizenberg, J., Weiner, S. & Addadi, L. (2003) *Connect. Tissue Res.* **44**, 20–25.
17. Beadle, W. E., Tsai, J. C. C. & Plummer, R. D. (1985) *Quick Reference Manual For Silicon Integrated Circuit Technology* (Wiley, New York).
18. Aizenberg, J., Tkachenko, A., Weiner, S., Addadi, L. & Hendler, G. (2001) *Nature* **412**, 819–822.
19. Ghatak, A. & Thyagarajan, K. (1998) *Introduction to Fiber Optics* (Cambridge Univ. Press, New York).
20. Clegg, W. J., Kendall, K., Alford, N. M., Button, T. W. & Birchall, J. D. (1990) *Nature* **347**, 455–457.
21. Mayer, G. & Sarikaya, M. (2002) *Exp. Mech.* **42**, 395–403.
22. Kamat, S., Su, X., Ballarini, R. & Heuer, A. H. (2000) *Nature* **405**, 1036–1040.
23. Smith, B. L., Schaffer, T. E., Viani, M., Thompson, J. B., Frederick, N. A., Kindt, J., Belcher, A., Stucky, G. D., Morse, D. E. & Hansma, P. K. (1999) *Nature* **399**, 761–763.
24. Morse, D. E. (1999) *Trends Biotechnol.* **17**, 230–232.
25. Shimizu, K., Cha, J., Stucky, G. D. & Morse, D. E. (1998) *Proc. Natl. Acad. Sci. USA* **95**, 6234–6238.
26. Cha, J. N., Shimizu, K., Zhou, Y., Christiansen, S. C., Chmelka, B. F., Stucky, G. D. & Morse, D. E. (1999) *Proc. Natl. Acad. Sci. USA* **96**, 361–365.
27. Kroger, N., Deutzmann, R., Bergsdorf, C. & Sumper, M. (2000) *Proc. Natl. Acad. Sci. USA* **97**, 14133–14138.
28. Kroger, N., Deutzmann, R. & Sumper, M. (1999) *Science* **286**, 1129–1132.
29. Kroger, N., Lorenz, S., Brunner, E. & Sumper, M. (2002) *Science* **298**, 584–586.
30. Cha, J. N., Stucky, G. D., Morse, D. E. & Deming, T. J. (2000) *Nature* **403**, 289–292.
31. Weaver, J. C. & Morse, D. E. (2003) *Microsc. Res. Tech.* **62**, 356–367.
32. Zhou, Y., Shimizu, K., Cha, J. N., Stucky, G. D. & Morse, D. E. (1999) *Angew. Chem. Int. Ed.* **38**, 779–782.
33. Parker, A. R., McPhedran, R. C., McKenzie, D. R., Botten, L. C. & Nicorovici, N.-A. P. (2001) *Nature* **409**, 36–37.
34. Vukusic, P. & Sambles, J. R. (2003) *Nature* **424**, 852–855.
35. Wilson, T. & Hastings, J. W. (1998) *Annu. Rev. Cell Dev. Biol.* **14**, 197–230.
36. Chamberlain, S. C. (2000) *Philos. Trans. R. Soc. London B* **355**, 1151–1154.
37. White, S. N., Chave, A. D., Reynolds, G. T., Gaidos, E. J., Tyson, J. A. & Van Dover, C. L. (2000) *Geophys. Res. Lett.* **27**, 1151–1154.